Positive Low Cloud Feedback Primarily Caused by Increasing Longwave Radiation from the Sea Surface in Two Versions of a Climate Model

Tomoo Ogura[1], Mark J. Webb[2], and Adrian P. Lock[2]

[1]National Institute for Environmental Studies, Tsukuba, Japan.

[2]Met Office Hadley Centre, Exeter, United Kingdom.

Corresponding author: Tomoo Ogura (ogura@nies.go.jp)

Key Points:

- The increase in longwave radiation from the sea surface is a leading order cause of the positive low cloud feedback in a climate model.

- This increase in longwave radiation leads to warming and drying in the boundary layer, which contributes to the decrease in the low cloud.

- This mechanism is not associated with increases in surface evaporation or vertical moisture contrast.

Abstract

Low cloud feedback in global warming projections by climate models is characterized by its positive sign, the mechanism of which is not well understood. Here we propose that the positive sign is primarily caused by the increase in upward longwave radiation from the sea surface. We devise numerical experiments that enable separation of the feedback into components coming from physically distinct causes. Results of these experiments with a climate model indicate that increases in upward longwave radiation from the sea surface cause warming and absolute drying in the boundary layer, leading to the positive low cloud feedback. The absolute drying results from decrease in surface evaporation, and also from decrease in inversion strength which enhances vertical mixing of drier free tropospheric air into the boundary layer. This mechanism is different from previously proposed understanding that positive low cloud feedback is caused by increases in surface evaporation or vertical moisture contrast.

Plain Language Summary

We project future climate change induced by atmospheric greenhouse gas increases by conducting numerical simulations using specialized computer codes, namely Global Climate Models. Results of such simulations are characterized by decreases in low cloud with warming at the Earth's surface, which amplifies the warming by reflecting less sunlight back to space and allowing more sunlight to be absorbed at the surface. This amplifying effect, called 'positive low cloud feedback', is important because the amount of future warming affects our living and safety. However, the mechanism of the low cloud decreases with warming is not well understood. Here we propose that the low cloud decrease is primarily caused by increase in upward longwave radiation from the sea surface. We devise numerical simulations that enable the separation of the low cloud feedback into components coming from physically distinct causes. Results of the simulations indicate that increases in upward longwave radiation from the sea surface cause warming and drying near the Earth's surface, leading to the low cloud decrease. This mechanism is different from previously proposed understanding that the low cloud decrease is due to increases in sea surface evaporation or vertical moisture contrast.

1 Introduction

Low cloud feedback is an important source of uncertainty in the projections of future climate using general circulation models (GCMs). The projections of future climate by multiple GCMs exhibit large inter-model differences, which cause difficulty in evaluating the impact of climate change. The inter-model difference in the projected surface air temperature for a given CO_2 increase is mainly attributable to the inter-model difference in cloud feedback (e.g., Caldwell et al. 2016; Vial et al. 2013; Webb et al. 2013). Specifically, changes in low cloud induced by surface warming make the largest contribution to this uncertainty (e.g., Zelinka et al. 2016, 2020). Understanding the inter-model difference in low cloud feedback is thus imperative, which motivates research on the mechanism of the low cloud feedback simulated by the GCMs.

An interesting feature of the low cloud feedback simulated by the GCMs is that it is positive in most models (Zelinka et al. 2020). The positive sign is associated with decreases in low cloud amount with surface warming, which amplifies the warming by allowing more solar radiation to be absorbed at the surface. However, the magnitude of the low cloud decrease varies widely across models, leading to a large uncertainty in the low cloud feedback. A critical

59 question here is why low cloud decreases with surface warming, the mechanism of which is not
60 well understood (Boucher et al. 2013; Forster et al. 2021).

61   Several studies have been conducted to address this issue by attributing simulated
62 changes in low cloud to changes in environmental factors (e.g., Qu et al. 2014, 2015b; Zhai et al.
63 2015; Myers and Norris 2016; Brient and Schneider 2016; McCoy et al. 2017; Klein et al. 2017;
64 Cesana and Del Genio 2021; Ceppi and Nowack 2021). Qu et al. (2014), among others,
65 developed a heuristic model which interprets the positive low cloud feedback in the subtropical
66 low cloud regions in GCMs. The model indicates that changes in low cloud amount mainly come
67 from two factors: local SST warming and increase in the strength of the inversion capping the
68 atmospheric boundary layer, which is measured by the Estimated Inversion Strength (EIS, Wood
69 and Bretherton 2006). The local SST warming tends to decrease low cloud, while the
70 enhancement of EIS tends to increase the cloud. The net effect is a decrease in low cloud amount
71 because the effect of the SST outweighs that of the EIS in most models.

72   The mechanism underlying the effect of EIS on low cloud is well understood (Klein and
73 Hartmann 1993; Wood and Bretherton 2006). However, the mechanism of how the local SST
74 warming influences the low cloud is still under debate. The following two mechanisms have
75 been proposed, based on studies using Large Eddy Simulations. First, SST warming leads to an
76 increase in surface latent heat flux, which enhances vertical mixing by turbulence or convection
77 in the lower troposphere. This enhances entrainment of drier air from the free troposphere into
78 the moister boundary layer, desiccating low cloud (Rieck et al. 2012). Second, the increase in
79 latent heat flux from the sea surface induces an increase in water vapor specific humidity in the
80 atmosphere. The magnitude of the increase in humidity is more pronounced in the boundary
81 layer than in free troposphere, increasing the vertical moisture contrast. This increase in moisture
82 contrast enhances the efficiency with which vertical mixing dehydrates the boundary layer,
83 reducing low cloud (Bretherton and Blossey 2014, Sherwood et al. 2014, van der Dussen et al.
84 2015).

85   Recently, however, detailed examination of some GCM experiments gave results which
86 are not consistent with the above understanding. For instance, Webb et al. (2018) explored the
87 impact of surface latent heat flux on low cloud amount, forcing the latent heat flux to increase at
88 different rates with SST warming in HadGEM2-A. They found that the magnitude of the low
89 cloud decrease becomes smaller when the latent heat flux is forced to increase at higher rates.
90 Similar results were obtained by Watanabe et al. (2018) using MIROC5. These findings suggest
91 that mechanisms other than the increase in latent heat flux are needed to explain the decrease in
92 low cloud with SST warming in climate models. However, such mechanisms are yet to be
93 identified. Here we propose an alternative mechanism for the low cloud decrease with SST
94 warming based on a new method for decomposing feedbacks in GCM experiments. We argue
95 that the increase in upward longwave radiation from the sea surface is a leading order cause of
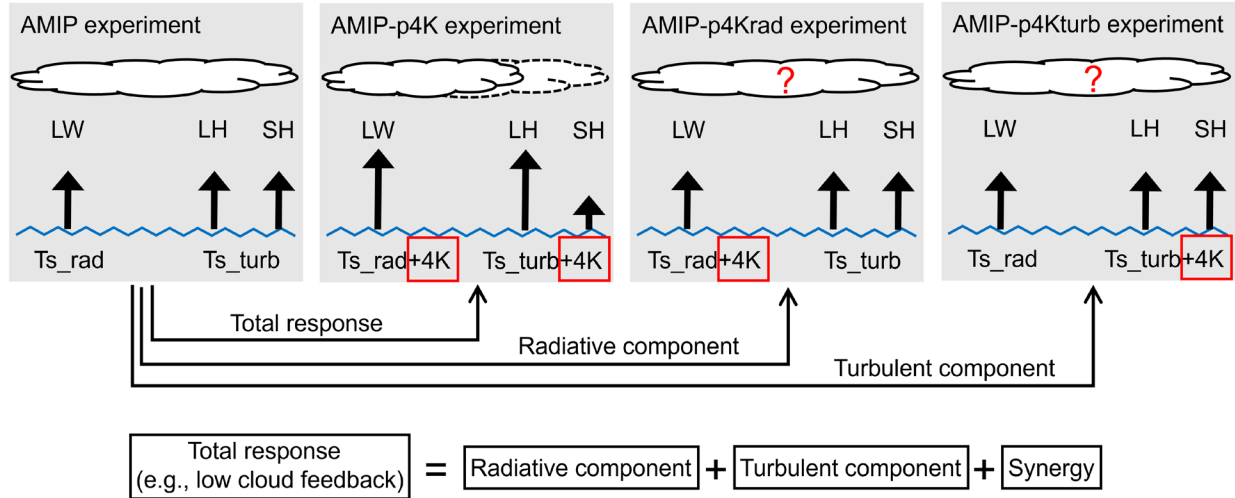96 the low cloud decrease.

Figure 1. Schematic showing the experimental design. Ts_rad indicates the SST used for calculating LW radiation from the sea surface. Ts_turb is the SST used for calculating turbulent transport from the sea surface, including latent heat (LH) and sensible heat (SH) fluxes.

2 Numerical experiments

The low cloud feedback is investigated using an atmospheric GCM MIROC6 with the spatial resolution of T85 ($\sim 1.4°$) with 81 vertical levels (Tatebe et al. 2019). The simulation protocol follows that of the Atmospheric Model Intercomparison Project (AMIP), in which the atmosphere is forced by a historical SST (AMIP experiment) and the SST uniformly warmed by 4K (AMIP-p4K experiment). The SSTs are not affected by the changes in the atmosphere since they are prescribed as a boundary condition. These AMIP-type experiments provide a good approximation to the cloud feedbacks determined from coupled atmosphere-ocean CO_2-forced simulations (Ringer et al. 2014; Qin et al. 2022).

In the AMIP-p4K run, the uniform SST warming of 4K compared to the AMIP run modifies the atmosphere via two causal pathways, firstly by increasing the upward longwave radiation from the sea surface, and secondly by changing the turbulent transport at the air-sea interface, such as the latent and sensible heat fluxes (Figure 1). The decrease in low cloud amount, and hence the positive low cloud feedback, is a result of these two causal factors.

We attempt to better understand the roles of the two factors by adding two experiments. In the first experiment, SST is raised by 4K only when calculating the upward longwave radiation from the sea surface using Planck function (AMIP-p4Krad experiment, Figure 1). In the second, SST is raised by 4K only when calculating the turbulent transport at the air-sea interface using bulk aerodynamic formulas (AMIP-p4Kturb experiment). More details of the two experiments are given in the Supporting Information (Text S1). All of the experiments are integrated for 1979-2014 and the output is averaged for 36 years.

The differences of the SST warming experiments compared to the AMIP run are called 'total response (AMIP-p4K minus AMIP)', 'radiative component (AMIP-p4Krad minus AMIP)', and 'turbulent component (AMIP-p4Kturb minus AMIP)', respectively. As the total response, we focus on the low cloud feedback, and write it as a sum of the radiative component, the turbulent

126 component, and a synergy term (Figure 1). Now the low cloud feedback is separated into
127 components that originate from physically distinct causes, namely, the effect of increasing SST
128 on upwelling surface longwave radiation and its effect on surface turbulent fluxes. The intention
129 here is to see which component makes the low cloud feedback positive. The synergy is a residual
130 term that is evaluated as the difference between the total response and the sum of the radiative
131 and turbulent components. It represents the effect of the radiative and turbulent components
132 working together.

133   All of the experiments, as outlined above, are repeated using another atmospheric GCM

134 MIROC5 with the spatial resolution of T42 (~2.8˚) with 40 vertical levels (Watanabe et al.

135 2010; Shiogama et al. 2012; Ogura et al. 2017). MIROC5 is different from MIROC6 in terms of
136 its representation of the atmospheric boundary layer. Specifically, MIROC5 does not include a
137 shallow convection parameterization while MIROC6 does. Still, the results from both models are
138 consistent with the main conclusions. For conciseness, we present results from MIROC6 in the
139 main part, while those from MIROC5 are shown in the Supporting Information (Figures S1-S2).

3 Results

141   We first present the low cloud feedback simulated by MIROC6 in Figure 2(a). This is
142 evaluated by multiplying changes in the ISCCP low cloud amount by the cloud radiative kernel,
143 which gives the changes in radiation flux at the TOA induced by the low cloud changes (Zelinka
144 et al. 2012; Bodas-Salcedo et al. 2011; Klein and Jakob 1999; Webb et al. 2001). The ISCCP
145 cloud amount with cloud top pressure greater than 680hPa is used for the evaluation. In Figure
146 2(a), we confirm that the global average low cloud feedback is positive. The positive signal is
147 particularly evident in subtropical marine regions off the western coasts of continents, where low
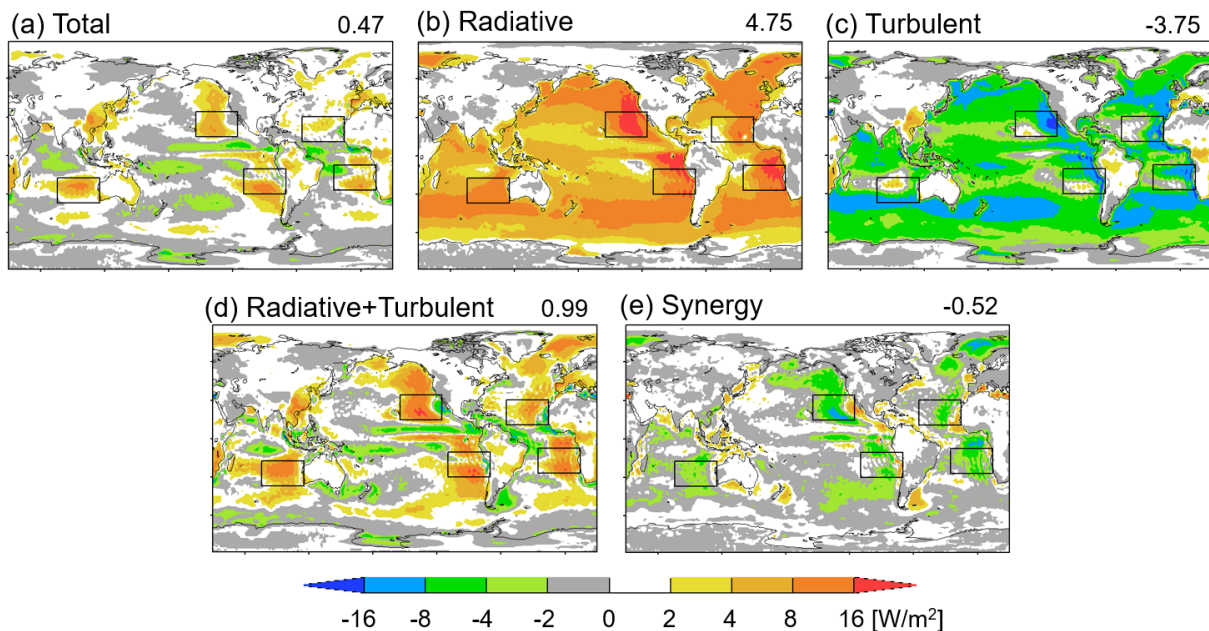148 clouds prevail in both observations and model control climates.

149

150

151   **Figure 2**. Low cloud feedback induced by 4K increases in SST. (a) Total low cloud feedback,
152   (b) radiative component, (c) turbulent component, (d) sum of the radiative and turbulent
153   components, and (e) synergy. Global averages are indicated at the top right of each panel. The
154   units can be converted to [W/m^2/K] by dividing by the surface warming of 4.54K in the AMIP-
155   p4K run. Black rectangles indicate low cloud regions focused on in Figure 3.

156

157   The low cloud feedback is separated into the radiative component, turbulent component,
158   and synergy as shown in Figure 2(b,c,e). The radiative component is characterized with positive
159   contributions over the oceans, while the turbulent component is dominated by negative
160   contributions (Figure 2b,c). If we add the two components together, as shown in Figure 2(d), the
161   result captures the geographical pattern (especially the sign) of the total low cloud feedback in
162   Figure 2(a). The pattern correlation between Figures 2(a) and 2(d) is 0.81. Therefore, the low
163   cloud feedback can be approximated as a sum of the radiative and turbulent components,
164   although the synergy effect is not negligible as shown in Figure 2(e).

165   Focusing on the sum of the radiative and the turbulent components in Figure 2(d), we
166   find that the low cloud feedback becomes positive where the radiative component outweighs the
167   turbulent component. Without the radiative component, the low cloud feedback would have been
168   negative overall (Figure 2c). This means that the low cloud feedback becomes positive because
169   of the radiative component. In other words, the positive sign of the feedback is mainly attributed
170   to the increase in upward longwave radiation from the sea surface. This argument applies to
171   MIROC5, too (Figure S1).

172   How does the longwave radiation cause the positive low cloud feedback? The mechanism
173   is further examined, focusing on area averages over the five oceanic regions indicated by the
174   black rectangles in Figure 2. These regions are chosen because the positive low cloud feedback
175   stands out here in MIROC6 (Figure 2a), and also because they match the low cloud regions
176   based on observations (Qu et al. 2014). Here, vertical profiles of cloud-related variables are
177   examined in Figure 3. We focus on the cloud amount below the 680hPa level because this is
178   where the low cloud feedback originates (Figure 3a,e). Note also that the low cloud feedback is
179   strongly correlated with the cloud amount, but less well with the cloud optical thickness or cloud
180   top pressure (Figure S3).

181   The total response of the cloud amount below the 680hPa level (Figure 3e, black) shows
182   a characteristic dipole pattern, in which a cloud decrease above (σ-p level$\approx$0.85) is moderated
183   by a cloud increase below (σ-p level$\gtrsim$0.9). The dipole pattern reflects shallowing of the
184   boundary layer cloud at σ-p level$\approx$0.9 (Figure 3a). As a comparison, we also plot the radiative
185   and turbulent components in Figure 3e (red and blue). Clearly, the turbulent component (blue)
186   fails to reproduce the total response (black) at the σ-p level$\gtrsim$0.9, namely, the blue curve
187   exceeds the black one. This explains how the turbulent component shows increase in low cloud,
188   leading to the negative feedback. In contrast, the radiative component (red) shows a decrease in
189   low cloud at σ-p level$\approx$0.9, which opposes the cloud increase in the turbulent component
190   (blue). When added together, the radiative and turbulent components (green) roughly reproduce
191   the dipole pattern in the total response (black), although the positive and negative maxima are

192 exaggerated. Hence, the low cloud decrease in the radiative component (red) is the key to
193 understanding the low cloud decrease in the total response (black).

194   The low cloud decrease in the radiative component (Figure 3e, red) is consistent with a
195 decrease in relative humidity (Figure 3f, red), which comes from both a warming and a decrease
196 in specific humidity (Figure 3gh, red). This can be confirmed by looking at the geographical
197 distribution (Figure S4). The warming is caused by the increase in upward longwave radiation
198 from the sea surface, which is absorbed by the atmosphere (Figure 3i). The decrease in specific
199 humidity can be explained by two mechanisms. Firstly, the magnitude of the warming is larger in
200 the boundary layer compared to the free troposphere, having a bottom-heavy vertical profile
201 (Figure 3h, red). This decreases the strength of the inversion capping the boundary layer. As a
202 result, vertical mixing across the inversion increases, making the boundary layer less humid
203 (Klein and Hartmann 1993). Secondly, the longwave-induced warming of the atmosphere
204 increases the static stability at the air-sea interface. Note that the SST is kept the same as the
205 AMIP experiment when calculating the turbulent transport at the air-sea interface in the AMIP-
206 p4Krad experiment. The increase in the static stability suppresses the turbulent transport of water
207 vapor from the sea surface, thereby contributing to the decrease in specific humidity (Text S2,
208 Figure S8).

209   The warming and the absolute drying in the boundary layer, as described above, leads to
210 the low cloud decrease in the radiative component. The mechanism may be summarized as
211 "Cloud Reduction due to Increased Surface Temperature Longwave Emission (CRISTLE)". In
212 addition, the decrease in the low cloud initiates a process that reduces the low cloud further.
213 Namely, the decrease in the low cloud causes weakening of the downward longwave radiation
214 from the cloud. As a result, divergence in the downward longwave radiation decreases, which
215 leads to weakening of the radiative cooling of the boundary layer (Figures S7c,f,i, blue). This
216 contributes to warming and a decrease in relative humidity, thereby reducing the low cloud
217 further (Figure S6e, green, Brient and Bony 2012). We note that the low cloud decrease in the
218 radiative component is not associated with an increase in specific humidity or surface
219 evaporation (Figures 3g, S8a). We also considered a number of other possible explanations for
220 the low cloud reductions in the radiative component (Table S1).

221   In the turbulent component, by contrast, the low cloud changes are associated with the
222 increase in specific humidity and surface evaporation. We attribute the low cloud increases in the
223 turbulent component to multiple processes that compete with each other (e.g., Wyant et al. 2009;
224 Vial et al. 2016; Tan et al. 2017; Schneider et al. 2019; Narenpitak and Bretherton 2019). For
225 instance, the magnitude of the increase in specific humidity is larger at lower altitudes, which
226 enhances the moisture contrast between the free troposphere and the boundary layer (Figure 3g,
227 blue). As a result, the upward moisture flux by shallow convection increases, which tends to
228 decrease the low cloud (Figures S5c,f, red, Zhang et al. 2013; Brient et al. 2016). In contrast, we
229 also note that the vertical temperature profile stabilizes with warming, which increases strength
230 of the inversion capping the boundary layer (Figure 3h, blue). As a result, vertical mixing across
231 the inversion reduces, which tends to keep the boundary layer more humid and increase the low
232 cloud (Miller 1997; Tan et al. 2016). Understanding the roles of different processes within the
233 turbulent component will be a subject of future studies. More details of the competing processes
234 are given in Table S1.

235   In the AMIP-p4Krad and the AMIP-p4Kturb experiments, the SST warming takes place
236 uniformly, including both the low cloud regions and the convective regions such as the western

237 tropical Pacific. Readers might be interested in whether the SST warming changes deep
238 convection, and whether the change in the deep convection has remote effects on the low clouds.
239 Our preliminary answer is "yes, to some extent".

240   In the AMIP-p4Kturb experiment, for instance, the SST warming leads to increase in
241 precipitation over the western tropical Pacific and the tropical Indian oceans (Figure S9c), which
242 is related to the enhanced latent heating by the deep convection. In the low cloud regions, at
243 700hPa level, temperature warms up by 4.8K (Figures S10c), which increases the EIS, and
244 subsidence weakens by 4.2hPa/day (Figures S11c). These are consistent with the understanding
245 that deep convection affects low clouds by changing the tropical overturning circulation and
246 temperature in the free troposphere (e.g., Williams et al. 2023; Schiro et al. 2022; Silvers and
247 Robinson 2021; Erfani and Burls 2019; Andrews and Webb 2018), and both the warming and the
248 weakening of subsidence will tend to increase the low clouds (e.g., Qu et al. 2015; Myers and
249 Norris 2013). Regarding the AMIP-p4Krad experiment, the SST warming leads to reduction of
250 precipitation over the western tropical Pacific and the tropical Indian oceans (Figure S9b), which
251 is related to suppressed latent heating by the deep convection. However, remote effects of the
252 changes in the deep convection are relatively small. In the low cloud regions, at 700hPa level,
253 temperature warms up by only 0.3K (Figure S10b) and subsidence weakens by only 1.0hPa/day
254 (Figure S11b). Those changes do not explain the decrease in the low cloud amount (Figure 3e,
255 red).

256   Then, what is the role of the local SST warming in the AMIP-p4Kturb experiment? Does
257 it decrease the low clouds, as indicated by the LES experiments? Currently, we have no answer
258 for this. Additional efforts are needed to separately quantify the local and remote effects of the
259 SST warming, which is a subject of future studies.

260   The results obtained so far illustrate how the low cloud feedback originates from the sea
261 surface warming. The processes involved in the feedback are classified into the radiative and the
262 turbulent components. The two components are dissimilar to each other, with the former
263 decreasing the ISCCP low cloud amount (LCA), while the latter increases it. However, the two
264 components are both related to changes in the EIS, as follows. In the radiative component, the
265 LCA decreases as the EIS decreases (Figure 3e,h, red). In the turbulent component, the LCA
266 increases as the EIS increases (Figure 3e,h, blue). In the synergy component, also, the LCA
267 increases as the EIS increases (not shown). The relationship between the LCA and the EIS is
268 qualitatively consistent with observation (Wood and Bretherton 2006).

269   If we add the three components together, however, the relation between the LCA and the
270 EIS changes compared to that above. Namely, the LCA decreases as the EIS increases (Figure
271 3e,h, black), which may appear counter-intuitive. Why does the relation between the LCA and
272 the EIS break down when the components are added together? This issue is examined in Figure
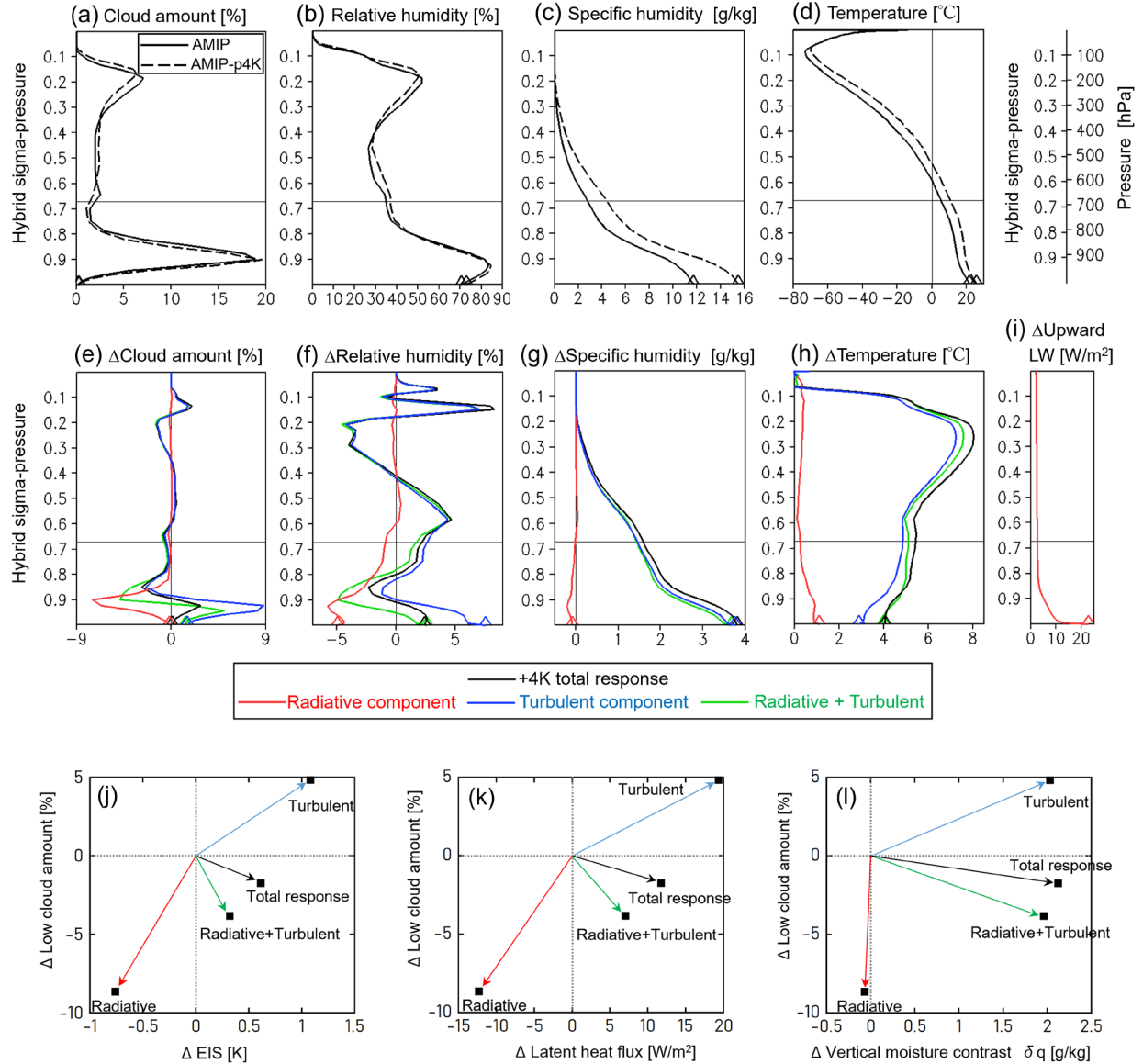273 3(j).

274

Figure 3. (a)-(i) Vertical profiles of cloud-related variables averaged over the low cloud regions in Figure 2. (a)(b)(c)(d) for AMIP and AMIP-p4K experiments, and (e)(f)(g)(h)(i) for changes due to +4K SST warming. The vertical coordinate is hybrid σ-p on model level, which is compared with pressure levels on the top-right corner. Horizontal lines at the σ-p level of 0.67 mark the boundary between low-top clouds and middle-top clouds at 680hPa. Diamonds indicate values at the lowest level. The changes in upward longwave, (i), are evaluated assuming that the atmosphere remains fixed at the AMIP condition. (j)-(l) Relationships between changes in low cloud amount and changes in (j) EIS, (k) latent heat flux, and (l) vertical moisture contrast δ q. The δ q is defined as the specific humidity q at 1000hPa minus q at 700 hPa. The delta, Δ,

285 denotes changes induced by the SST warming of 4K. The data are averages over the low cloud
286 regions in Figure 2.

287

288 In figure 3(j), the changes induced by the SST warming of 4K are represented by 2-D
289 vectors on the ΔEIS-ΔLCA plane. The radiative component is shown in red, with the coordinate
290 values of $(\Delta EIS_{rad}, \Delta LCA_{rad})$, while the turbulent component is shown by blue, with the
291 coordinate values of $(\Delta EIS_{turb}, \Delta LCA_{turb})$. The two vectors appear in the 3rd and the 1st
292 quadrants, indicating that the LCA decreases (increases) as the EIS decreases (increases). Adding
293 the two components together, we obtain the sum shown by green, with the coordinate values of
294 $(\Delta EIS_{turb} + \Delta EIS_{rad}, \Delta LCA_{turb} + \Delta LCA_{rad})$. Now the vector appears in the 4th quadrant,
295 indicating that the LCA decreases as the EIS increases, which captures the sign of the total
296 response shown in black.

297 Focusing on the sum of the two components, we find that the LCA decreases as the EIS
298 increases under the following conditions:

299 $$\Delta EIS_{turb} + \Delta EIS_{rad} > 0 \text{ , and } \Delta LCA_{turb} + \Delta LCA_{rad} < 0 \qquad (1).$$

300 Namely, the change in the EIS is dominated by the turbulent component, while the change in the
301 LCA is dominated by the radiative component. In other words, the total response to the SST
302 warming includes two counter-acting components, and which component dominates depends on
303 the variable we look at. This explains how the relation between the LCA and the EIS changes
304 when adding the radiative and turbulent components together.

305 We also note that rate of change in the LCA with respect to the EIS is different between
306 the radiative and turbulent components, as follows:

307 $$\Delta LCA_{rad}/\Delta EIS_{rad} > \Delta LCA_{turb}/\Delta EIS_{turb} \qquad (2).$$

308 The conditions (1) can be met only under the condition (2). The condition (2) indicates that LCA
309 is less sensitive to EIS in the turbulent component than in the radiative component. This may be
310 because, in the turbulent component, the EIS increase is accompanied by an increase in vertical
311 moisture contrast, δq (Figure 3gh, blue). The change in the EIS tends to increase the LCA,

312 while the change in the δq tends to decrease it, making the LCA less sensitive to the EIS

313 (Kawai et al. 2017).

314 Similar arguments hold, even if we replace the EIS with the surface latent heat flux or the
315 vertical moisture contrast, δq (Figure 3k,l). Namely, in the total response shown in black, the

316 LCA decrease is accompanied by an increase in latent heat flux or δq. This can be explained by

317 the fact that the LCA decrease is dominated by the radiative component while the increase in
318 latent heat flux or δq is driven by the turbulent component.

319 **4 Conclusions**

320 In order to understand the reason for the positive sign of the low cloud feedback
321 simulated by GCMs, we devise numerical experiments which enable separation of the feedback
322 into three components, namely, the effect of increasing SST on upwelling surface longwave

radiation, its effect on surface turbulent fluxes, and the synergy between the two. The numerical experiments are conducted using MIROC5 and MIROC6. The results indicate that the positive sign of the low cloud feedback is mainly attributed to the increase in longwave radiation from the sea surface, which leads to a warming and a drying in the boundary layer, as well as a decrease in the low cloud amount (LCA). The mechanism involved is summarized as "Cloud Reduction due to Increased Surface Temperature Longwave Emission (CRISTLE)". It is not associated with increases in surface latent heat flux or vertical moisture contrast. The decomposition of the feedback also helps to explain how the LCA decrease is accompanied by increases in the EIS, the latent heat flux, and the vertical moisture contrast.

The present study mainly discusses the positive low cloud feedback over the subtropical oceans off the western coast of the continents. If we broaden the scope, however, we find other regions where the low cloud feedback becomes negative due to changes in the surface turbulent fluxes. There are also regions where the synergy exceeds sum of the radiative and the turbulent terms. Therefore, the geographical pattern of the low cloud feedback on the global scale is determined by the changes in the upward surface longwave radiation and the turbulent fluxes, as well as their interaction. We also note that the low cloud feedback simulated in the present study includes contribution from the SST warming in regions remote from the low cloud. This contribution from the remote SST warming appears to be a major factor in the turbulent component.

Whether other GCMs or Large Eddy Simulations support the present findings will be an interesting topic for future studies. Currently, output from CMIP6 experiments is analyzed to see if the mechanism proposed in this study can explain the sub-tropical low cloud feedbacks in multi-GCMs. In addition, the experiments proposed in this study are being conducted with a Large Eddy Simulation model under the CGILS protocol (Blossey et al. 2016). The results will be presented in subsequent papers.

Open Research

Data used in this study are available at https://doi.org/10.5281/zenodo.4153249 (Ogura and Webb 2020).

References

Andrews, T. and M. J. Webb (2018), The dependence of global cloud and lapse rate feedbacks on the spatial structure of tropical Pacific warming, *J. Clim.*, 31, 641-654, doi:10.1175/JCLI-D-17-0087.1.

Blossey, P. N., C. S. Bretherton, A. Cheng, S. Endo, T. Heus, A. P. Lock, and J. J. van der Dussen (2016), CGILS Phase 2 LES intercomparison of response of subtropical marine low cloud regimes to CO_2 quadrupling and a CMIP3 composite forcing change, *J. Adv. Model. Earth Syst.*, 08, doi:10.1002/2016MS000765.

Boucher, O., D. Randall, P. Artaxo, C. Bretherton, G. Feingold, P. Forster, V. -M. Kerminen, Y. Kondo, H. Liao, U. Lohmann, P. Rasch, S. K. Satheesh, S. Sherwood, B. Stevens, and X. Y. Zhang (2013), Clouds and Aerosols. In:*Climate Change 2013:The Physical Science Basis. Contribution of Working Group 1 to the Fifth Assessment Report of the Intergovernmental Panel on Climate Change* [Stocker, T. F., D. Qin, G. -K. Plattner, M. Tignor, S. K. Allen, J. Boschung, A. Nauels, Y. Xia, V. Bex, and P. M. Midgley (eds.)]. Cambridge University Press, Cambridge, United Kingdom and New York, NY, USA.

Bodas-Salcedo, A., M. J. Webb, S. Bony, H. Chepfer, J. -L. Dufresne, S. A. Klein, Y. Zhang, R. Marchand, J. M. Haynes, R. Pincus, and V. O. John (2011), COSP Satellite simulation software for model assessment, *Bull. Amer. Meteor. Soc.*, 92, 1023–1043, doi:10.1175/2011BAMS2856.1.

Bretherton, C. S., P. N. Blossey, and C. R. Jones (2013), Mechanisms of marine low cloud sensitivity to idealized climate perturbations: A single-LES exploration extending the CGILS cases, J. Adv. Model. Earth Syst., 5, 316-337, doi:10.1002/jame.20019.

Bretherton, C. S. and P. N. Blossey (2014), Low cloud reduction in a greenhouse-warmed climate: Results from Lagrangian LES of a subtropical marine cloudiness transition, *J. Adv. Model. Earth Syst.*, 6, doi:10.1002/2013MS000250.

Brient, F. and S. Bony (2012), How may low-cloud radiative properties simulated in the current climate influence low-cloud feedbacks under global warming? *Geophys. Res. Lett.*, 39, L20807, doi:10.1029/2012GL053265.

Brient, F. and S. Bony (2013), Interpretation of the positive low-cloud feedback predicted by a climate model under global warming, Clim. Dyn., 40, 2415-2431, doi:10.1007/s00382-011-1279-7.

Brient, F. and T. Schneider (2016), Constraints on climate sensitivity from space-based measurements of low-cloud reflection, *J. Clim.*, 29, 5821–5835, doi:10.1175/JCLI-D-15-0897.1.

Brient, F., T. Schneider, Z. Tan, S. Bony, X. Qu, and A. Hall (2016), Shallowness of tropical low clouds as a predictor of climate models' response to warming, Clim. Dyn., 47, 433-449, doi:10.1007/s00382-015-2846-0.

Caldwell, P. M., M. D. Zelinka, K. E. Taylor and K. Marvel (2016), Quantifying the sources of intermodal spread in equilibrium climate sensitivity, *J. Clim.*, 29, 513–524, doi:10.1175/JCLI-D-15-0352.1.

Ceppi, P., and P. Nowack (2021), Observational evidence that cloud feedback amplifies global warming, *Proc. Natl. Acad. Sci. U.S.A.*, 118, 30, e2026290118, doi:10.1073/pnas.2026290118.

Cesana, G. V., and A. D. Del Genio (2021), Observational constraint on cloud feedbacks suggests moderate climate sensitivity, *Nat. Clim. Change*, 11, 213-218, doi:10.1038/s41558-020-00970-y.

Erfani, E. and N. J. Burls (2019), The strength of low-cloud feedbacks and tropical climate: A CESM sensitivity study, *J. Clim.*, 32, 2497-2516, doi:10.1175/JCLI-D-18-0551.1.

Forster, P., T. Storelvmo, K. Armour, W. Collins, J.-L. Dufresne, D. Frame, D. J. Lunt, T. Mauritsen, M. D. Palmer, M. Watanabe, M. Wild, and H. Zhang (2021), The Earth's Energy Budget, Climate Feedbacks, and Climate Sensitivity. In *Climate Change 2021: The Physical Science Basis. Contribution of Working Group 1 to the Sixth Assessment Report of the Intergovernmental Panel on Climate Change* [Masson-Delmotte, V., P. Zhai, A. Pirani, S. L.

Connors, C. Péan, S. Berger, N. Caud, Y. Chen, L. Goldfarb, M. I. Gomis, M. Huang, K.

Leitzell, E. Lonnoy, J. B. R. Matthews, T. K. Maycock, T. Waterfield, O. Yelekçi, R. Yu, and B.

Zhou (eds.)]. Cambridge University Press, Cambridge, United Kingdom and New York, NY, USA, pp.923-1054, doi:10.1017/9781009157896.009.

Kawai, H., T. Koshiro, and M. J. Webb (2017), Interpretation of factors controlling low cloud cover and low cloud feedback using a unified predictive index, *J. Clim.*, 30, 9119-9131, doi:10.1175/JCLI-D-16-0825.1.

Klein, S. A., and D. L. Hartmann (1993), The seasonal cycle of low stratiform clouds, *J. Clim.*, 6, 1587–1606.

Klein, S. A., and C. Jakob (1999), Validation and sensitivities of frontal clouds simulated by the ECMWF model, *Mon. Wea. Rev.*, 127, 2514–2531.

Klein, S. A., A. Hall, J. R. Norris, and R. Pincus (2017), Low-cloud feedbacks from cloud-controlling factors: a review, *Surv. Geophys.*, 38, 1307–1329, doi:10.1007/s10712-017-9433-3.

McCoy, D. T., R. Eastman, D. L. Hartmann, and R. Wood (2017), The change in low cloud cover in a warmed climate inferred from AIRS, MODIS, and ERA-Interim, *J. Clim.*, 30, 3609-3620, doi:10.1175/JCLI-D-15-0734.1.

Miller, R. L. (1997), Tropical thermostats and low cloud cover, *J. Clim.,* 10, 409-440.

Myers, T. A., and J. R. Norris (2013), Observational evidence that enhanced subsidence reduces subtropical marine boundary layer cloudiness, *J. Clim.*, 26, 7507-7524, doi:10.1175/JCLI-D-12-00736.1.

Myers, T. A., and J. R. Norris (2016), Reducing the uncertainty in subtropical cloud feedback, *Geophys. Res. Lett.*, 43, doi:10.1002/2015GL067416.

Narenpitak, P., and C. S. Bretherton (2019), Understanding negative subtropical shallow cumulus cloud feedbacks in a near-global aquaplanet model using limited area cloud-resolving simulations, *J. Adv. Model. Earth Syst.,* 11, 1600-1626, doi:10.1029/2018MS001572.

Ogura, T., and M. J. Webb (2020), Atmospheric responses to partial SST perturbations simulated by MIROC5 and 6 [Dataset], Zenodo, https://doi.org/10.5281/zenodo.4153249.

Ogura, T., H. Shiogama, M. Watanabe, M. Yoshimori, T. Yokohata, J. D. Annan, J. C. Hargreaves, N. Ushigami, K. Hirota, Y. Someya, Y. Kamae, H. Tatebe, and M. Kimoto (2017), Effectiveness and limitations of parameter tuning in reducing biases of top-of-atmosphere

radiation and clouds in MIROC version 5, *Geosci. Model Dev.*, 10, 4647-4664, doi:10.5194/gmd-10-4647-2017.

Qin, Y., M. D. Zelinka, and S. A. Klein (2022), On the correspondence between atmosphere-only and coupled simulations for radiative feedbacks and forcing from CO_2, *J. Geophys. Res. Atmos.*, 127, e2021JD035460, doi:10.1029/2021JD035460.

Qu, X., A. Hall, S. A. Klein, and P. M. Caldwell (2014), On the spread of changes in marine low cloud cover in climate model simulations of the 21st century, *Clim. Dyn.*, 42, 2603–2626, doi:10.1007/s00382-013-1945-z.

Qu, X., A. Hall, S. A. Klein, and P. M. Caldwell (2015), The strength of the tropical inversion and its response to climate change in 18 CMIP5 models, *Clim. Dyn.*, 45, 375-396, doi:10.1007/s00382-014-2441-9.

Qu, X., A. Hall, S. A. Klein, and A. M. DeAngelis (2015b), Positive tropical marine low-cloud cover feedback inferred from cloud-controlling factors, *Geophys. Res. Lett.*, 42, 7767–7775, doi:10.1002/2015GL065627.

Rieck, M., L. Nuijens, and B. Stevens (2012), Marine boundary layer cloud feedbacks in a constant relative humidity atmosphere, *J. Atmos. Sci.*, 69, 2538–2550, doi:10.1175/JAS-D-11-0203.1.

Ringer, M. A., T. Andrews, and M. J. Webb (2014), Global-mean radiative feedbacks and forcing in atmosphere-only and coupled atmosphere-ocean climate change experiments, *Geophys. Res. Lett.,* 41, doi:10.1002/2014GL060347.

Schiro, K. A., H. Su, F. Ahmed, N. Dai, C. E. Singer, P. Gentine, G. S. Elsaesser, J. H. Jiang, Y. -S. Choi, and J. D. Neelin (2022), Model spread in tropical low cloud feedback tied to overturning circulation response to warming, *Nat. Commun.*, 13, 7119, doi:10.1038/s41467-022-34787-4.

Schneider, T., C. M. Kaul, and K. G. Pressel (2019), Possible climate transitions from breakup of stratocumulus decks under greenhouse warming, Nat. Geosci., 12, 163-167, doi:10.1038/s41561-019-0310-1.

Sherwood, S. C., S. Bony, and J. -L. Dufresne (2014), Spread in model climate sensitivity traced to atmospheric convective mixing, *Nature*, 505, 37–42, doi:10.1038/nature12829.

Shiogama, H., M. Watanabe, M. Yoshimori, T. Yokohata, T. Ogura, J. D. Annan, J. C. Hargreaves, M. Abe, Y. Kamae, R. O'ishi, R. Nobui, S. Emori, T. Nozawa, A. Abe-Ouchi, and M. Kimoto (2012), Perturbed physics ensemble using the MIROC5 coupled atmosphere-ocean GCM without flux corrections: experimental design and results -parametric uncertainty of climate sensitivity, *Clim. Dyn.*, 39, 3041–3056, doi:10.1007/s00382-012-1441-x.

Silvers, L. G. and T. Robinson (2021), Clouds and radiation in a mock-Walker circulation, *J. Adv. Model. Earth Syst.*, 13, e2020MS002196, doi:10.1029/2020MS002196.

Tatebe, H., T. Ogura, T. Nitta, Y. Komuro, K. Ogochi, T. Takemura, K. Sudo, M. Sekiguchi, M. Abe, F. Saito, M. Chikira, S. Watanabe, M. Mori, N. Hirota, Y. Kawatani, T. Mochizuki, K. Yoshimura, K. Takata, R. O'ishi, D. Yamazaki, T. Suzuki, M. Kurogi, T. Kataoka, M. Watanabe, and M. Kimoto (2019), Description and basic evaluation of simulated mean state,

internal variability, and climate sensitivity in MIROC6, *Geosci. Model Dev.*, 12, 2727–2765, doi:10.5194/gmd-12-2727-2019.

Tan, Z., T. Schneider, J. Teixeira, and K. G. Pressel (2016), Large-eddy simulation of subtropical cloud-topped boundary layers: 1. A forcing framework with closed surface energy balance, *J. Adv. Model. Earth Syst.*, 8, 1565-1585, doi:10.1002/2016MS000655.

Tan, Z., T. Schneider, J. Teixeira, and K. G. Pressel (2017), Large-eddy simulation of subtropical cloud-topped boundary layers: 2. Cloud response to climate change, *J. Adv. Model. Earth Syst.*, 9, 19-38, doi:10.1002/2016MS000804.

van der Dussen, J. J., S. R. de Roode, S. Dal Gesso, and A. P. Siebesma (2015), An LES model study of the influence of the free tropospheric thermodynamic conditions on the stratocumulus response to a climate perturbation, *J. Adv. Model. Earth Syst.*, 7, 670–691, doi:10.1002/2014MS000380.

Vial, J., J. -L. Dufresne, and S. Bony (2013), On the interpretation of inter-model spread in CMIP5 climate sensitivity estimates, *Clim. Dyn.*, 41, 3339–3362, doi:10.1007/s00382-013-1725-9.

Vial, J., S. Bony, J.-L. Dufresne, and R. Roehrig (2016), Coupling between lower-tropospheric convective mixing and low-level clouds: Physical mechanisms and dependence on convection scheme, *J. Adv. Model. Earth Syst.*, 8, 1892-1911, doi:10.1002/2016MS000740.

Vogel, R., L. Nuijens, and B. Stevens (2019), Influence of deepening and mesoscale organization of shallow convection on stratiform cloudiness in the downstream trades, Q. J. R. Meteorol. Soc., 146, 174-185, doi:10.1002/qj.3664.

Watanabe, M., T. Suzuki, R. O'ishi, Y. Komuro, S. Watanabe, S. Emori, T. Takemura, M. Chikira, T. Ogura, M. Sekiguchi, K. Takata, D. Yamazaki, T. Yokohata, T. Nozawa, H. Hasumi, H. Tatebe, and M. Kimoto (2010), Improved climate simulation by MIROC5: mean states, variability, and climate sensitivity, *J. Clim.*, 23, 6312–6335, doi:10.1175/2010JCLI3679.1.

Watanabe, M., Y. Kamae, H. Shiogama, A. M. DeAngelis, and K. Suzuki (2018), Low clouds link equilibrium climate sensitivity to hydrological sensitivity, *Nat. Clim. Change*, 8, 901–906, doi:10.1038/s41558-018-0272-0.

Webb, M. J., C. Senior, S. Bony, and J. -J. Morcrette (2001), Combining ERBE and ISCCP data to assess clouds in the Hadley Centre, ECMWF, and LMD atmospheric climate models, *Clim. Dyn.*, 17, 905–922.

Webb, M. J., F. Hugo Lambert, and J. M. Gregory (2013), Origins of differences in climate sensitivity, forcing and feedback in climate models, *Clim. Dyn.*, 40, 677–707, doi:10.1007/s00382-012-1336-x.

Webb, M. J. and A. P. Lock (2013), Coupling between subtropical cloud feedback and the local hydrological cycle in a climate model, Clim. Dyn., 41, 1923-1939, doi:10.1007/s00382-012-1608-5.

Webb, M. J., A. P. Lock, and F. Hugo Lambert (2018), Interactions between hydrological sensitivity, radiative cooling, stability, and low-level cloud amount feedback, *J. Clim.*, 31, 1833–1850, doi:10.1175/JCLI-D-16-0895.1.

524 Williams, A. I. L., N. Jeevanjee, and J. Bloch-Johnson (2023), Circus tents, convective
525 thresholds, and the non-linear climate response to tropical SSTs, *Geophys. Res. Lett.*, 50,
526 e2022GL101499, doi:10.1029/2022GL101499.

527 Wood, R., and C. S. Bretherton (2006), On the relationship between stratiform low cloud cover
528 and lower-tropospheric stability, *J. Clim.*, 19, 6425–6432, doi:10.1175/JCLI3988.1.

529 Wyant, M. C., C. S. Bretherton, and P. N. Blossey (2009), Subtropical low cloud response to a
530 warmer climate in a superparameterized climate model. Part 1: Regime sorting and physical
531 mechanisms, *J. Adv. Model. Earth Syst.,* 1, 7, doi:10.3894/JAMES.2009.1.7.

532 Zhai, C., J. H. Jiang, and H. Su (2015), Long-term cloud change imprinted in seasonal cloud
533 variation: More evidence of high climate sensitivity, *Geophys. Res. Lett.*, 42, 8729-8737,
534 doi:10.1002/2015GL065911.

535 Zhang, M., C. S. Bretherton, P. N. Blossey, P. H. Austin, J. T. Bacmeister, S. Bony, F. Brient, S.
536 K. Cheedela, A. Cheng, A. D. Del Genio, S. R. De Roode, S. Endo, C. N. Franklin, J.-C. Golaz,
537 C. Hannay, T. Heus, F. A. Isotta, J.-L. Dufresne, I.-S. Kang, H. Kawai, M. Köehler, V. E.
538 Larson, Y. Liu, A. P. Lock, U. Lohmann, M. F. Khairoutdinov, A. M. Molod, R. A. J. Neggers,
539 P. Rasch, I. Sandu, R. Senkbeil, A. P. Siebesma, C. Siegenthaler-Le Drian, B. Stevens, M. J.
540 Suarez, K.-M. Xu, K. von Salzen, M. J. Webb, A. Wolf, and M. Zhao (2013), CGILS: Results
541 from the first phase of an international project to understand the physical mechanisms of low
542 cloud feedbacks in single column models, *J. Adv. Model. Earth Syst.*, 5, 1-17,
543 doi:10.1002/2013MS000246.

544 Zelinka, M. D., S. A. Klein, and D. L. Hartmann (2012), Computing and partitioning cloud
545 feedbacks using cloud property histograms. Part I:cloud radiative kernels, *J. Clim.*, 25, 3715-
546 3735, doi:10.1175/JCLI-D-11-00248.1.

547 Zelinka, M. D., C. Zhou, and S. A. Klein (2016), Insights from a refined decomposition of cloud
548 feedbacks, *Geophys. Res. Lett.*, 43, doi:10.1002/2016GL069917.

549 Zelinka, M. D., T. A. Myers, D. T. McCoy, S. Po-Chedley, P. M. Caldwell, P. Ceppi, S. A.
550 Klein, and K. E. Taylor (2020), Causes of higher climate sensitivity in CMIP6 models. *Geophys.
551 Res. Lett.*, 47, e2019GL085782. doi:10.1029/2019GL085782.

552
553